A Preliminary Report on a Full-Body Imaging System for Effectively Collecting and Processing Biometric Traits of Prisoners

Nhat Quang Huynh, Xingpeng Xu, Adams Wai Kin Kong
School of Computer Engineering
Nanyang Technological University, Singapore
{nqhuynh, xpxu, adamskong}@ntu.edu.sg

Sathyan Subbiah*
Department of Mechanical Engineering
Indian Institute of Technology Madras, India
sathyans@iitm.ac.in

***Abstract*—Because of recent advances in imaging technology, the use of image-based evidences, such as faces and tattoos, is increasing dramatically. Face and tattoo images of prisoners are collected regularly for suspect image database establishment. New biometric traits such as skin marks, androgenic hairs, and blood vessels hidden in color images are getting more attention because they are shown to be useful for criminal and victim identification, especially when their faces and tattoos are neither observable nor available. The current manual approach of collecting images of prisoners is extremely time consuming and does not record these new biometric traits. To address this problem, an unprecedented full-body imaging system is developed. Furthermore, an automatic and systematic routine based on the system for effectively collecting prisoners' images is proposed. This paper concentrates on the system hardware design as well as its image collecting and processing capability. The system has been used to collect and process more than 30,000 infrared and color images from 188 subjects. Its performance is very encouraging.**

Keywords—criminal and victim identification; tattoo; child porn; prisoners' image database establishment

I. INTRODUCTION

Recent technological advances have allowed for a proliferation of the use of image-based evidence, such as in cases of child sexual offenses, violent protests and acts of terrorism. The U.S. Customs Service estimated that around 100,000 websites are involved with child pornography [1]. From 2002 to 2008, in Canada alone, approximately 30,000 child pornography cases were reported [2]. Furthermore, because of economic and political instability in the last several years, many cities and countries, including Rome, Athens, London, Bahrain, Turkey and Thailand, experienced violent protests. Terrorist acts also disrupt normal life in many parts of the world. Nowadays, digital cameras are everywhere, so such illegal activities can be easily recorded and the images can be found on the Internet. Images of terrorists can also be obtained because many are interviewed by reporters. However, pedophiles in child pornographic images, violent protestors, and terrorists always cover or hide their faces to avoid being identified. Only some parts of their bare skin are usually available. Tattoos come in handy in those cases [3], but they are neither unique nor always available. To further address these identification problems, skin marks, blood vessel patterns hidden in color images, and androgenic hair patterns have been proposed [4-6]. These research results indicate that many characteristics on the skin are useful for criminal and victim identification.

Currently, law enforcement agents record face and tattoo images of every prisoner to form suspect databases. These databases are often used to search for suspects because ex-prisoners in the first several years of their release have greater risk of committing another crime [8]. Several methods have been developed to match photofits with face images in these databases [9]. If the faces of criminals are observable in evidence images, commercial face recognition systems can be used directly. Prisoners' tattoos are annotated manually. There are some standards to annotate tattoos (e.g., ANSI/NIST-ITL 1-2000 [10]). Such textual information has been used for tattoo retrieval for many years. Recently, techniques developed for content-based image retrieval have been applied to tattoo retrieval [11-12]. Some researchers attempt to match sketches with tattoo images [13]. These methods require well processed input tattoo images. Fig. 1 shows some typical examples, in which the tattoos occupy most of the space, required by these methods. However, when tattoo images are collected from prisoners, they always contain a lot of other information (e.g., face, shorts, arms and background) that may influence retrieval results. Fig. 2 gives three stimulated examples.

To use skin marks, scars, androgenic hair patterns, and blood vessel patterns for searching suspects, they must also be collected regularly from prisoners. A small experiment was carried out to simulate the routine of an officer capturing images of these biometric traits, including faces and tattoos, from different body sites of a prisoner as in Fig. 5, renaming the images, saving them into a database, labelling the positions of the tattoos on the body, and segmenting the face and tattoos. This tedious process takes approximate more than an hour for one prisoner. In 2012, the numbers of prisoners in USA and China were 2.02 million and 1.55 million respectively [19]. Therefore, if this image collection process is carried on manually for all the prisoners, an enormous amount of time, manpower and money will be required.

*All his work for this paper was done at Nanyang Technological University, Singapore.

To address this problem, we developed a full-body imaging system together with a routine for effectively collecting and processing images from prisoners. As a result, the required time is reduced significantly. The raw images are renamed and stored into a database automatically. Furthermore, these raw images, which each contains a part of the body, are stitched together to form a full-body image. Then, an algorithm is applied to the full-body image to detect the joints. Based on the mapping between the raw images and the full-body image as well as the coordinates of the joints, if a tattoo or any other biometric trait is spotted, its location on the body can be defined. This geometric information can be used for criminal and victim search. Fig. 3 illustrates the relationships between the proposed full-body imaging system and other related research works. According to our best knowledge, no such computational method or system has been developed especially for effectively collecting and processing images of prisoners before.

Due to the space constraint, this paper only concentrates on the hardware of the system, the image collection routine, the raw image preprocessing and the tattoo detection. The other parts will be presented in a future paper. The rest of this paper is organized as follows. Section 2 presents the system design and the routine. Section 3 describes the image stitching algorithm and the joint detection algorithm. Section 4 discusses the tattoo detection algorithm for the images collected by the system. Section 5 reports the experimental results. Finally, Section 6 offers some conclusive remarks.

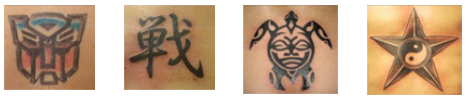

Fig. 1. Typical tattoo images demanded by current tattoo retrieval methods. Most of the space is occupied by the tattoos.

Fig. 2. Prisoner tattoo images often contain other information hindering tattoo detection and matching. (Simulated images)

II. The System Design and the Routine

To record the biometric traits, including faces, tattoos, skin marks, scars, blood vessels, and androgenic hair patterns of prisoners effectively, the hardware components are built carefully to achieve the stability, best quality images and user friendly interaction. The image collection routine takes advantage of the hardware components to capture almost every inch of the skin of a prisoner.

A. The Hardware Components

The system composes mainly of a consumer camera, a near infrared (NIR) camera, infrared light sources, visible light sources, an actuator and a background with uniform color. Black is chosen as the background color so that images taken by the NIR camera can be easily segmented later. Because the resolutions of commercially available consumer and NIR cameras are not enough to capture the whole body with clear skin marks in one single image, an actuator is used to move the cameras vertically to take multiple images. The actuator, the consumer camera and the NIR camera are connected to a computer. Fig. 4 shows different views of the system. A small software component is developed to control the two cameras and the actuator. Once the height of a prisoner, which determines the positions of the images being taken, is inputted to the system, the rest of the image collection process is completely automatic.

B. The Image Collection Routine

A prisoner is photographed at six different poses, which are illustrated in Fig. 5. Nearly all body sites can be captured, including the inner and outer sides of arms and legs. Only the sides of the upper body and some minor parts are left out. The actuator moves up from the bottom and stops at the height of the prisoner's face. The number of images being taken depends on the prisoner's height. For each camera, two consecutive images from the same pose are shot at the heights with 20 cm difference. Each image taken by the consumer camera has a corresponding image taken at the same position by the NIR camera. Thus, vein patterns visualized from color images, e.g., evidence images can be compared with the vein patterns in the NIR images [6]. Images collected from the same pose are overlapping, which allows image processing methods to combine them into a full-body image.

With this routine, none of the valuable data will be missed out. Fig. 6 shows the collected biometric traits. Mugshots can be obtained by applying a face detection method to the top image collected from the front pose. Fig. 7 shows four mugshots captured by the system.

If the height of a prisoner is between 160 cm and 179 cm, 8 images per camera per pose will be captured. If the height is between 180 cm and 200 cm, 9 images per camera per pose will be captured. On average, a person will have either 96 or 108 images, including color and NIR images taken in one collection. If all these images are collected and their files are renamed manually, it takes an hour for processing the data from one person. The proposed system taking only 9 minutes to perform all these tasks reduces time consuming and manpower cost significantly.

Some may suggest that multiple consumer cameras and NIR cameras should be installed on a vertical bar and therefore, they can take images of different body sites simultaneously. Though this approach can save some time, it has two drawbacks. The cameras always capture images at the same positions, regardless of the height of prisoners. Human height of adults can vary substantially from 60 cm to 250 cm [14-15]. If the cameras are not installed dense enough, some important biometric traits, e.g., faces may be broken into two images (Fig. 8). To avoid this problem, a large number of cameras are required, which leads to the increase of the system cost. This approach is thus much more expensive than the one presented in this paper.

The system has been used to collect images from 188 volunteers; 145 of them are male. Fig. 5 shows a set of images from a subject. The height of the subjects is between 149 cm and 189 cm. All the images were saved with well-defined file names based on the poses, user identity numbers and body sites. This makes up a database of more than 30,000 images.

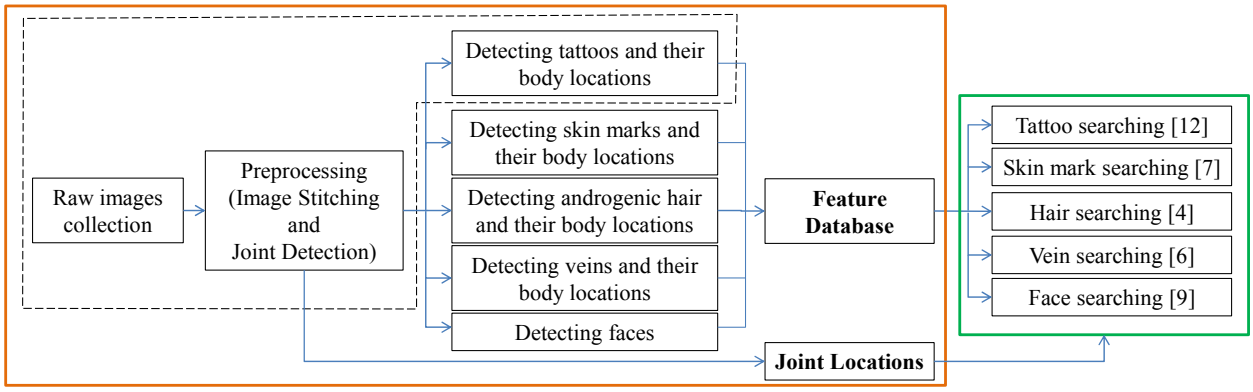

Fig. 3. Illustration of the relationships between the proposed full-body imaging system and other related research works. The orange rectangle covers all the modules of this system while the black dot line indicates the parts reported in this paper.

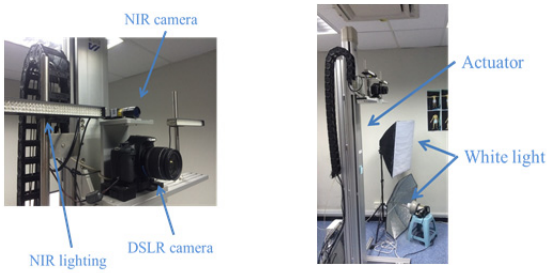

Fig. 4. Different views of the proposed imaging system.

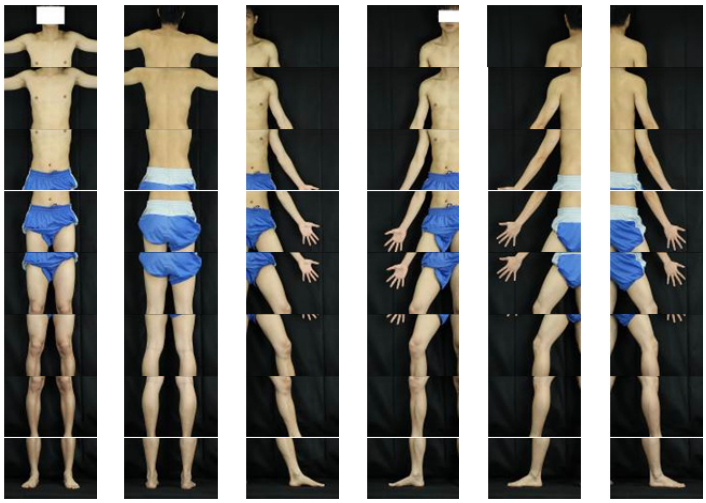

Fig. 5. Six sequences of color images collected from different poses.

Fig. 6. Various biometric traits collected by the full-body imaging system: face, tattoo, skin mark, scar, blood vessel, and androgenic hair. (From left to right).

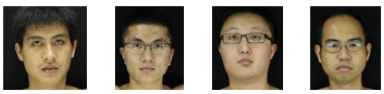

Fig. 7. Mugshots produced by the full-body imaging system.

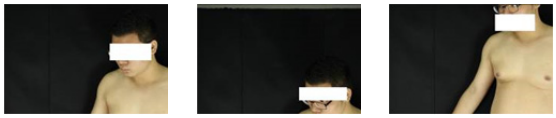

Fig. 8. Illustrating a potential problem of an alternative approach which uses fixed-position cameras to take images. The first image is collected by the proposed system. The second and third images are simulated images collected by the alternative approach.

III. The Image Stitching Algorithm and the Joint Detection Algorithm

This section presents an image stitching algorithm and a joint detection algorithm, which are used to label the locations of the biometric traits. The image stitching algorithm is utilized to stitch the overlapping raw images collected from the same pose into a full-body image. The mapping of the full-body image from the raw images is retained. Each pose of each subject has a full-body image from which the joints are detected by a joint detection algorithm. As long as all the joints are detected, their coordinates in the full-body image can be projected back to the corresponding raw images based on the mapping. Thus, the coordinates of the joints in the raw images can also be determined. As a result, if a trait is spotted on a raw image, its location in the full body can be defined. Given the location of a particular query trait from an eye witness or an evidence image, this query trait will only be matched with the ones on the same body location in a suspect database. Therefore, these two algorithms can help law enforcement agents save a lot of searching time and reduce the searching range. With the proposed system, no manual operations will be required to label the positions of tattoos and other biometric traits.

A. The Image Stitching Algorithm

With the setup mentioned in Section 2, each pair of consecutive images captured by the same camera is overlapping. Thus, a manifold projection algorithm can be employed to perform image mosaic [16-17]. Each raw color image with the size of 4,752 × 3,168 pixels is reduced to 5% of its original size and changed to grayscale to speed up the stitching speed. The bicubic interpolation is used to resize the images because it gives better stitching results than the linear

interpolation. A directed graph G (Fig. 10a) is formed by the rows of images in the same pose. Each image has n nodes, where n is the image height. The weights between nodes in the same image are defined as

$$w_{ij} = \begin{cases} 0.01, & if\ j = i + 1 \\ \infty, & otherwise \end{cases}. \quad (1)$$

Each pair of consecutive images (A, B) has an overlapping area, so node i of image A connects to node j of image B only if both nodes i and j belong to the same overlapping area. To travel from node i of image A to node j of image B, node i must be as similar as node $(j\text{-}1)$ because the transition from node $(j\text{-}1)$ to node j should be the smoothest. Let A_i be the matrix formed from row $(i\text{-}3)$ to row $(i+3)$ of image A and B_{j-1} be the matrix formed from row $(j\text{-}4)$ to row $(j+2)$ of image B. The weight q_{ij} for traveling from node i to node j is $||A_i - B_{j-1}||_2$. However, the subjects may shake when the cameras are on the move. Thus, horizontal shifted matching between A_i and B_{j-1} is performed. More clearly, B_{j-1} is shifted to left and right in a range of ten pixels to compare to A_i. Let A_i^x and B_{j-1}^x be A_i and B_{j-1} after B_{j-1} is shifted to x pixels and both A_i and B_{j-1} are patched with zeros to make them have equal length. The weight q_{ij} for traveling from node i to node j now becomes

$$q_{ij} = min_{x\in[-10\ 10]} ||A_i^x - B_{j-1}^x||_2. \quad (2)$$

The optimal way to stich images in one pose is the shortest path to travel from the first node to the last node of the graph G. The output image is approximately 630 × 240 pixels. The algorithm works well on our database and no obvious artifact is noted. For each subject, the algorithm produces 6 full-body color images for the six poses. The first two images in Fig. 9 are results given by the algorithm.

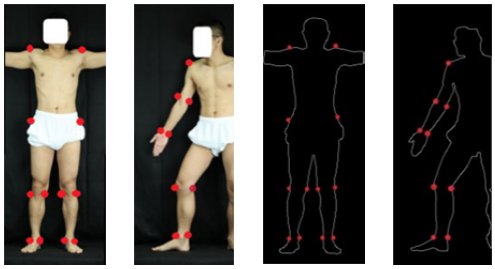

Fig. 9. Full-body images (the first and second) are produced by the image stitching algorithm. The third and fourth images show the boundaries extracted from the first and second images respectively. The red dots are the detected joints.

B. The Joint Detection Algorithm

Once the full-body image is obtained, it is converted into a grey image for joint detection. An adaptive threshold algorithm is applied to produce a binary image, from which the boundary of the body can be extracted. However, if the skin of the subject is too dark, the obtained boundary will not be smooth and may affect the results of joint detection. Hence, a skin segmentation scheme is developed to extract the skin pixels correctly. Because different color and materials of backgrounds were tested when designing the system, the red channels of skin images always have high values and the skin segmentation process becomes very simple. The red (R) and green (G) channels of the resized images are first separated. If ($t_1 < R(x,y) - G(x,y) < t_2$), where t_1 and t_2 are two predefined thresholds, the corresponding pixel is regarded as a skin pixel; otherwise, it is considered as a non-skin pixel. The skin pixels and the non-skin pixels form a binary image. Then, a morphological filling operation is applied to provide a smooth segmentation result. Finally, the body boundary image and the skin image are combined to obtain a perfect body boundary. The last two images in Fig. 9 show two body boundaries of the front pose and the side pose. Because prisoners will be well posed under instructions of prison officers, their joints can be detected easily.

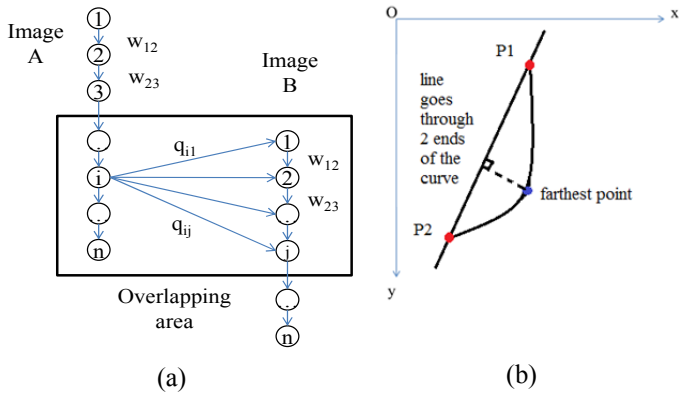

Fig. 10. (a) Illustration of the graph G built by the stitching algorithm. (b) Illustration of the process to detect a joint point at the location with large curvature.

A generic algorithm illustrated in Fig. 10b is designed to detect most of the joints, because many of them have large curvature. Firstly, a segment of the body boundary around a joint is extracted. Then, a line is constructed to connect the two end points of the segment. The distances between each point of the curve and the line are calculated. Finally, the point, which its distance from the curve is maximum, is regarded as the joint point. However, if this maximum distance is less than a threshold t, the curve is considered a straight line and the joint point cannot be detected. This can happen in the detection of knee and elbow points of the side poses. Exception handling is performed and discussed in separated paragraphs.

The detection processes of each joint in front and back pose images are given below.

- The shoulder points: The armpits can be detected by the algorithm given above because of their large curvature. The points on the boundary right above the armpits are regarded as the shoulder points. Fig. 11a illustrates the process to detect the right shoulder point.
- The hip points: The points on the boundary at half the distance between the head and the foot are marked as the hip points.
- The knee points: According to the anatomy study [18], the distance from knees to soles is a quarter of the person's height. Using this information, the knee points on the boundary of both legs are detected.
- The ankle points: Firstly, the outermost point on the right foot boundary is detected. Secondly, a point on

the outer boundary of the right leg and below the knee is selected. The curve connecting these two points is obtained and the outer ankle of right leg is detected by the algorithm given above. Then, the inner ankle point of the right leg can also be detected easily. This process is illustrated in Fig. 11b. The same process is applied to determinate the ankle points of the left leg.

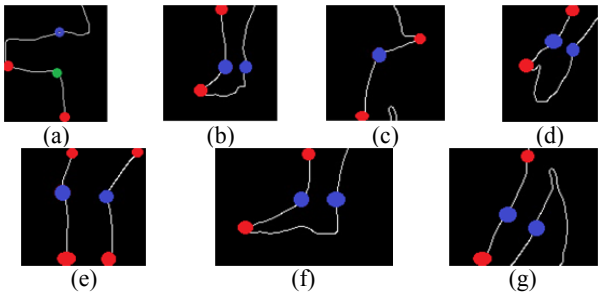

Fig. 11. (a)-(b) illustrate respectively the shoulder and ankle point detection in the front pose image. (c)-(g) illustrate respectively the shoulder, wrist, knee, ankle and elbow detection processes in the side pose images. The blue dots are the joint points, the red dots are the end points of the curves around the joints and the green dot is the armpit.

For the side pose images, which show the full upper and lower limbs, the shoulders, the elbows, the wrists, the knees, and the ankles are detected. The detection processes of these joints in the right side pose images are given below. The processes of detecting joints in the left side pose images are almost the same. For the space limit, they are not mentioned.

- The shoulder points: Firstly, a point on the outer boundary of the upper arm is selected. Next, from this point, the outer boundary of the upper arm is travelled upward and the largest x-coordinate of the point on the boundary is kept tract. If there is a decline in the value of the x-coordinate and the difference between the newest x-coordinate and the largest x-coordinate is greater than four pixels, the point with the largest x-coordinate is regarded as the neck point. Based on the starting point and the detected neck point, the shoulder point can be detected by the algorithm given above. Fig. 11c illustrates this process to detect the right shoulder point in the side pose image.
- The wrist points: Firstly, the outermost point on the right hand boundary is detected. Secondly, a point on the outer boundary of the right forearm is selected. Same as other joint points, the outer wrist point can be detected by the algorithm given above. Then, the inner wrist point can also be detected easily. Fig. 11d illustrates this detection process.
- The knee points: The boundary curves around the knee are extracted. Then, the algorithm is used to detect the knee point in the right curve (Fig. 11e). If the joint point cannot be determined, the algorithm is applied again to the left curve (Fig.11e). If the joint point is still not determined, a pair of points on the two curves, which has minimum distance, is selected as the knee points.
- The ankle points: The same detection process applied to front pose images is also employed to detect the ankle points in the side pose images. Fig. 11f illustrates it.
- The elbow points: The algorithm is not sufficient to detect the elbow points in the case that the subject keeps his/her arm straight. Thus, the ratio of the distance between the elbow and the shoulder to the distance between the wrist and the shoulder is used to perform the detection. Fig. 11g illustrates this process.

IV. Tattoo Detection for Prisoners' Images

Though the system captures various biometric traits, this paper concentrates on only tattoos because they have been regularly used by law enforcement agents and the current tattoo retrieval methods depend on processed tattoo images (Fig. 1).

Fig. 12 illustrates the proposed tattoo detection algorithm for prisoners' images. It uses a multiresolution approach to detect tattoos with different sizes. For large tattoos, an input color image collected by the consumer camera with size of 4,752 × 3,168 pixels is resized to 297 × 198 pixels for edge detection, and then the edge image is resized again to 594 × 396 pixels for searching large tattoo candidates. For small tattoos, the same input image is resized to 832 × 555 pixels and this image size is used in all the operations. The same image processing steps illustrated in Fig. 12 are applied to both cases except for the step of resizing the edge images.

To obtain the skin portions in an image, the skin segmentation method mentioned in the joint detection algorithm section is employed again. This simple method works well for all our color images, which are half of 30,000 images in our database. Because the system is used in control environments, the images in the database do not suffer from variations of lighting conditions. Our database contains images from many different races, including Chinese, Indian, Japanese, Indonesian, Malaysian, Mexican and European. Their skin colors are very diverse.

To extract edges in the segmented skin, a local adaptive threshold operation is applied. Mathematically, it can be described by

$$K(x,y) = \delta(M_w(x,y) - R_s(x,y) - t_3) \quad (3)$$

where R_s is the red channel of the segmented skin image, whose non-skin pixel values are zero, M_w is a resultant image by applying a median filter with a size of $w \times w$ to R_s, $t_3 \in \mathbb{R}$ is a threshold and δ is a unit step function. For large tattoos, K is resized to 594 × 396 pixels and for small tattoos, K is resized to 832 × 555 pixels. Morphological opening and thinning operators are applied to the resized K. An edge density image is obtained through counting the number of local edge pixels and it is binarized and smoothed to obtain tattoo candidates. The tattoo candidates can be real tattoos, but can also be body sites with strong edges, e.g., androgenic hair and nipples.

The tattoo candidates are passed to a classification scheme illustrated in Fig. 13. Firstly, the tattoo candidates are divided into overlapping blocks with size of 25 × 25 pixels. For clear

illustration, Fig. 13 shows only non-overlapping blocks. Then, features listed below are extracted from each block.

- The edge orientation histograms.
- The length of the longest edge.
- The mean of the length of the top three longest edges.
- The total number of edge pixels.
- The four 8-bin histograms from the R, G and B channels and the grayscale image.
- The difference between the number of elements in the bin having the greatest number of elements in the R (Cr) channel and those in the B (Cb) channel.
- The means of the R, G and B channels and the grayscale image.
- The difference between the standard derivations of the R and B channels.
- The difference between the standard derivations of the Cr and Cb channels from the YCrCb space.
- The covariance matrix of the R, G and B values.
- The mean and standard deviation of the grayscale image.

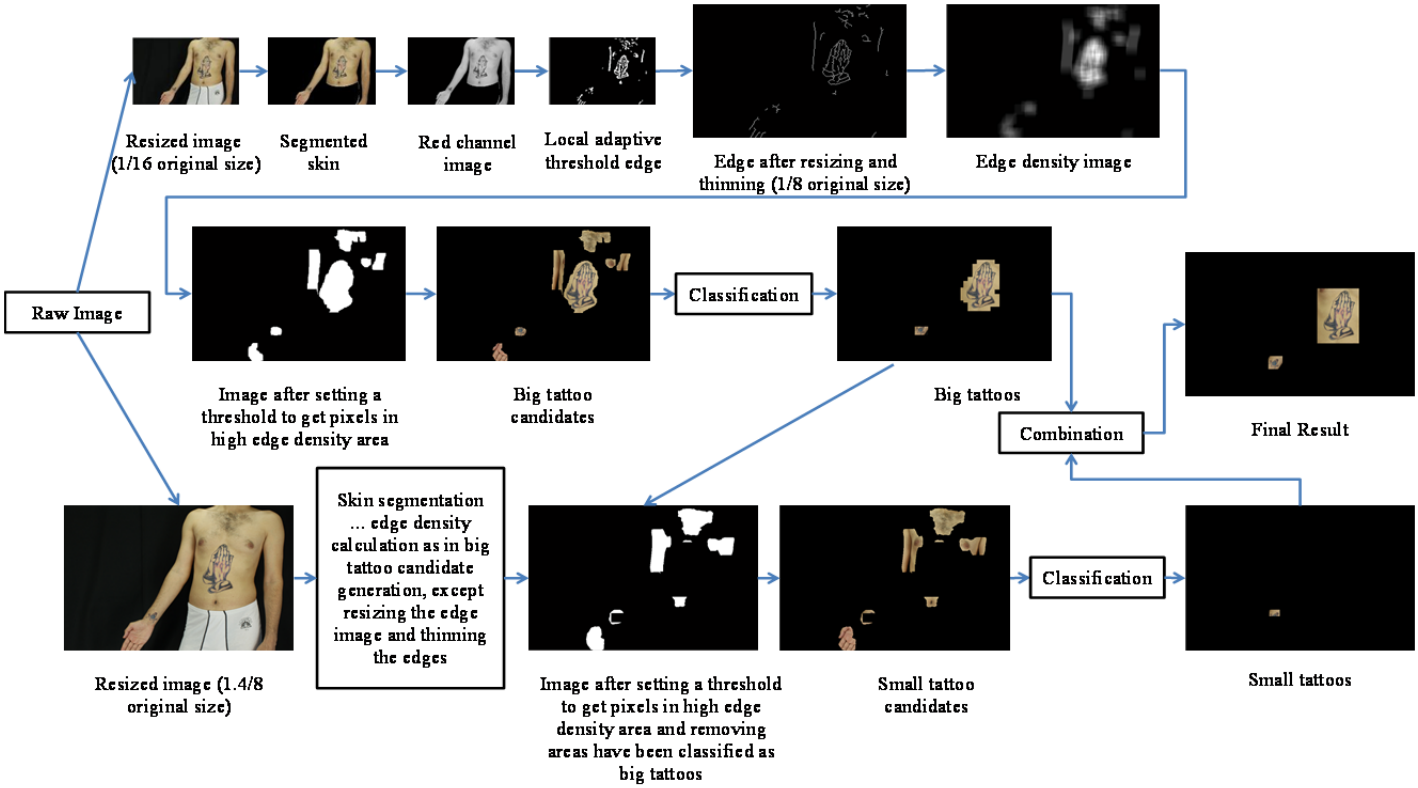

Fig. 12. A schematic diagram to illustrate the proposed tattoo detection algorithm.

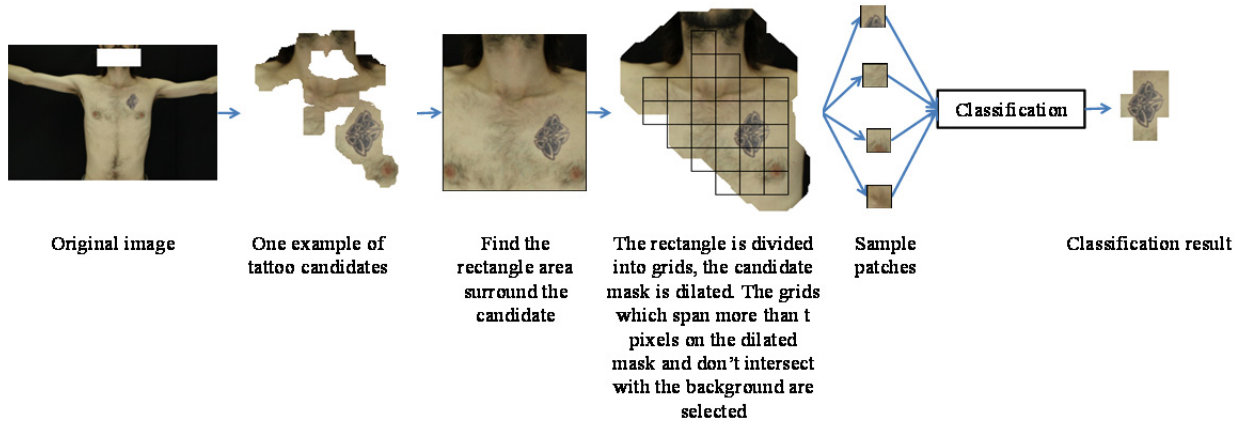

Fig. 13. Illustration of the classification scheme that is used to separate tattoos and other skin characteristics, e.g., hair.

One hundred decision trees are used to form an ensemble for this classification and Adaboost is used to enhance the classification performance. As with other classification systems, our classification scheme also makes mistakes. To correct these mistakes, some prior knowledge is used. If a block is classified as a tattoo block, but none of its neighboring block is classified as a tattoo block, it will still be considered as a non-tattoo block. The classification results from the two scales, one for large tattoo detection and the other for small tattoo detection, are combined into one image and bounding boxes are generated for the detected tattoos. Finally, they are extracted and stored in a tattoo database.

V. Experimental Results

A. The Joint Detection Algorithm

To evaluate the joint detection algorithm, we invited 5 testers to manually mark the joint points on 180 images, including 6 poses of 30 subjects. The average Euclidean distances between the automatically detected joint points and the manually marked joint points as well as the average Euclidean distances between manually marked joint points from different testers are calculated. The results are reported in Tables 1 and 2. The detection results are acceptable when comparing to the full-body image size of 630 x 240 pixels. The largest distances happen at the hip points, where the testers usually marked at the waistband of the shorts, not at half the height of the subject like the designed algorithm.

TABLE I. Average Euclidean Distances between Automatic Detected Points and Manual Marked Points as well as among Manual Marked Points from Different Testers of Front and Back Poses.

		Front		Back	
		Mean	***Std***	***Mean***	***Std***
Auto to Manual	Shoulder	7.35	4.82	9.73	3.75
	Hip	15.81	5.96	15.26	5.26
	Knee	14.25	5.84	8.50	2.84
	Ankle	9.55	3.83	8.97	3.36
Manual to Manual	Shoulder	6.85	3.43	7.05	2.71
	Hip	3.23	1.46	2.73	1.05
	Knee	2.77	1.34	2.91	1.04
	Ankle	2.40	0.99	2.73	1.13

TABLE II. Average Euclidean Distances between Automatic Detected Points and Manual Marked Points as well as among Manual Marked Points from Different Testers of Side Poses.

		Left Front		Right Front		Left Back		Right Back	
		Mean	***Std***	***Mean***	***Std***	***Mean***	***Std***	***Mean***	***Std***
Auto to Manual	Shoulder	5.39	2.22	5.89	3.26	6.75	3.51	7.34	2.50
	Elbow	7.83	3.54	7.48	2.30	8.10	3.58	6.90	3.23
	Wrist	4.67	2.48	5.00	1.53	4.63	1.06	3.75	1.16
	Knee	6.86	3.39	7.64	3.49	8.04	3.09	6.98	3.62
	Ankle	7.17	3.23	9.43	3.44	9.19	3.23	8.48	3.69
Manual to Manual	Shoulder	3.65	1.05	4.48	1.73	5.12	2.00	5.54	1.21
	Elbow	2.88	1.50	3.15	1.25	3.09	1.28	3.26	1.43
	Wrist	2.33	0.83	2.85	1.32	2.78	1.30	2.56	1.22
	Knee	2.38	1.06	2.57	1.17	2.62	1.21	2.39	0.86
	Ankle	2.91	1.16	2.39	0.95	2.56	1.03	2.75	1.25

Fig. 9 shows the detected joints in a front pose image and a side pose image. The algorithm was tested on a database of 653 images of front and back poses and 1306 images of side poses. It only failed to detect a shoulder point in one side pose image and a knee point in another side pose image. The first case is because the subject did not follow the pose instructions and placed his head very close to his shoulder, which makes the boundary around the shoulder become a straight line. The second case is because the subject's black short covered the area near his knee, which makes the algorithm detect the wrong curves around the knee. In real imaging environments, prisoners should wear uniform and under strict pose instructions so these errors should not happen.

B. The Tattoo Detection Algorithm

As mentioned in Section 2, the system has been used to collect more than 30,000 images. Only two subjects have tattoos on their upper arms and backs, the rest of them do not have any tattoos because they are mainly students who came from Asian countries. So, tattoos collected from the Internet were added on the original images of 107 subjects by Photoshop. Tattoos which embrace the whole arms or legs are not considered. 1,937 synthetic tattoo images, whose colors are diverse, were generated. In total, including real and synthetic tattoo images, there are 1,943 tattoo images.

Fig. 14 shows a sequence of synthetic tattoo images from one subject. The same tattoo was carefully added in the image sequences to simulate images collected from a subject with the tattoo. One tattoo usually appears in 9 images. These 1,943 tattoo images were mixed with non-tattoo images to form a testing database with 5,069 images, on which the proposed tattoo detection algorithm was examined. 10,000 tattoo blocks and 10,000 non-tattoo blocks, which were randomly extracted from another skin image database with real tattoos, were used to train the classification scheme. Note that this skin image database was not collected by the proposed system. Note also that the training and testing databases were disjointed.

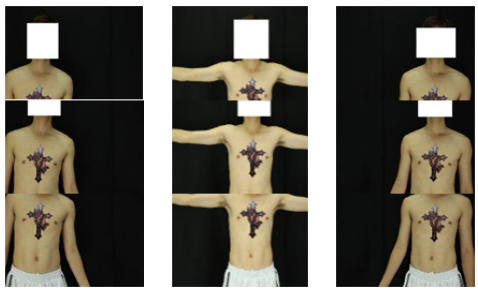

Fig. 14. Synthetic tattoo images in an image sequence.

TABLE III. Detection Accuracy in Terms of the Number of Subjects

	One Tattoo	**Two Tattoos**	**Three Tattoos**	**More Than 3**
Number of Subject	25	61	14	7
All Full Tattoos Are Detected	25	61	14	6
Accuracy	100	100	100	85.71

The proposed algorithm successfully detected 97.27% tattoos in the tattoo images. The undetected tattoos were usually very small and appeared at the skin borders or the image borders. The algorithm incorrectly recognized other skin features as tattoos in 1.41% non-tattoo images. Fig. 15 shows some successful detection. The detection rate of 97.27% does not describe the true performance because one tattoo appeared

Fig. 15. Some successful results given by the proposed tattoo detection algorithm.

in more than one image (Fig. 14). When a full tattoo (e.g., the tattoos in the second and the third rows of Fig. 14) was detected in one of the images in the sequences, it could be regarded as a successful detection. However, when only a fragment of the tattoo (e.g., the tattoos in the first row of Fig. 14) was detected, the detection could not be counted. Table 3 shows the detection accuracy in terms of the number of subjects. The 1st to 3rd columns show the results of the subjects with one to three tattoos respectively, which the algorithm correctly detected all tattoos. The last column shows the results of the subjects with more than three tattoos. It made one mistake, where one tattoo could not be detected. The overall detection accuracy in terms of the number of subjects is 99.07% and in terms of the number of tattoos is 99.55%.

VI. Conclusion

To effectively collect biometric traits, including faces, tattoos, skin marks, scars, androgenic hair and blood vessels, from prisoners, a full-body imaging system is developed and an image collection routine is introduced. The system reduces the image collection time significantly. To pre-process the collected images, an image stitching algorithm is used and a joint detection algorithm is developed for automatically labelling the locations of the biometric traits. Besides, a tattoo detection algorithm is proposed to enable the system for automatic tattoo database construction. The processed tattoo images given by the algorithm are demanded by other tattoo retrieval methods and are more effective even for manual search. Using an existing face detection method, mugshot databases are also constructed automatically. We will continually increase functionalities of this system, e.g., using the positional information given by the joint detection algorithm for tattoo retrieval.

Acknowledgment

This work is partially supported by the Ministry of Education, Singapore through Academic Research Fund Tier 2, MOE2012-T2-1-024.

References

[1] BBC News, “International child porn ring smashed”, 26 March 2001. Available: http://news.bbc.co.uk/1/hi/world/americas/1244457.stm.

[2] Canada’s National Tipline for Reporting the Online Sexual Exploitation of Children. Available: http://www.cybertip.ca/pdfs/fact_sheet_pdfs/English/CyberStats_en.pdf.

[3] G.E. Cains, and R.W. Byard, The forensic and cultural implications of tattooing. Forensic Pathology Review 5, Springer, 97–220, 2008.

[4] H. Su and A.W.K. Kong. An evaluation on low resolution androgenic hair patterns for criminal and victim identification. IEEE TIFS, 9(4):666–680, 2014.

[5] A. Nurhudatiana, A.W.K. Kong, K. Matinpour, D. Chon, L. Altieri, S.Y. Cho and N. Craft. The individuality of relatively permanent pigmented or vascular skin marks (RPPVSM) in independently and uniformly distributed patterns. IEEE TIFS, 8(6):998–1012, 2013.

[6] H. Zhang, C. Tang, A.W.K. Kong, and N. Craft. Matching vein patterns from color Images for forensic investigation. BTAS, 77–84, 2012.

[7] A. Nurhudatiana, A.W.K. Kong, L. Altieri and N. Craft Automated identification of relatively permanent pigmented or vascular skin marks (RPPVSM). ICASSP, 2984–2988, 2013.

[8] A. Blumstein and K. Nakamura. Redemption in the presence of widespread criminal background checks. Criminology, 47(2):327–359, 2009.

[9] P.C. Yuen and C.H. Man. Human face image searching system using sketches. IEEE Transactions on SMC, Part A, 37(4):493–504, 2007.

[10] ANSI/NIST-ITL 1-2000 standard: American National Standard for Information Systems - Data Format for the Interchange of Fingerprint, Facial, & Scar Mark & Tattoo (SMT) Information, 1993.

[11] J.E. Lee, A.K. Jain and R. Jin. Scars, marks and tattoos (SMT): soft biometric for suspect and victim identification. Biometrics Symposium, September, 1–8, 2008.

[12] A.K. Jain, J.E. Lee and R. Jin. Tattoo-ID: automatic tattoo image retrieval for suspect and victim identification. Proc. of the Multimedia 8th Pacific Rim Conference on Advances in Multimedia Information Processing, 256–265, 2007.

[13] H. Han and A.K. Jain. Tattoo based identification: sketch to image matching. ICB, 2013.

[14] Shortest persons ever declared: Chandra Bahadur Dangi. Huffington Post 27, February, 2012.

[15] World’s tallest man over 8ft high. BBC News, 17 September, 2009.

[16] S. Peleg and J. Herman. Panoramic mosaics by manifold projection. CVPR, 338–343, 1997

[17] Q. Zhi, and J.R. Cooperstock. Toward dynamic image mosaic generation with robustness to parallax. IEEE TIP, 21(1):366–378, 2012.

[18] B. Hermann. Anatomie des Menschen: ein Lehrbuch für Studierende und Ärzte. 1921.

[19] NationMaster, “All countries compared for Crim > Prisoners”, The Eight United Nations Survey on Crime Trends and the Operations of Criminal Justice System, 2002. Available: http://www.nationmaster.com/country-info/stats/Crime/Prisoners